Proceedings of the Institute of Acoustics

SYNTHETIC APERTURE IMAGING AND AUTOFOCUS WITH COHERENT MIMO SONAR SYSTEMS

Yan Pailhas OSL, Heriot Watt University, Edinburgh, UK
Yvan Petillot OSL, Heriot Watt University, Edinburgh, UK

1 INTRODUCTION

MIMO stands for Multiple Inputs Multiple Outputs. Such systems have received a lot of interests in the radar community during the last decade[1] . One of the main reason behind this is the greater variety in terms of target view angles compared with traditional monostatic systems. With several independent views one can hope to reduce the speckle effect typical of coherent sensor systems such as RADAR or SONAR. Destructive interference in particular can be the cause of missed detection. MIMO sonar systems have been studied by the ASW[2,3] (anti-submarine warfare) community mainly to increase the probability of detection of low strength target. Few MIMO systems have been built and tested including DEMUS (LF SIMO system built by CMRE). In any case all those systems use a relatively low number of sensors.

With coherent large MIMO systems we demonstrated[4] that with a sufficient number of independent views it is possible to solve the speckle within one resolution cell. Using back projection algorithm super-resolution imaging is then archivable making such systems very attractive for area surveillance. In this paper we study the practicality of large MIMO systems and in particular the sensors location accuracy needed to perform coherent processing. We propose a MIMO calibration method to solve the transducer location uncertainty. The independent view assumption places constraints on the MIMO design[5] especially on the sensor locations. The sensor locations are then extremely sparse compared to a $\lambda/2$ phased array and the sidelobes can be significant.

In a second part of this paper we discuss sidelobe reduction for MIMO imaging using randomised sensor positioning. Finally we propose two MIMO autofocus techniques to estimate with great accuracy mid-water target depth, speed and orientation. All the MIMO data in this paper are computed using a full 3D realistic MIMO simulator[6] including multipath, seabed physical models and cloud point model to compute time echoes. For the simulations the MIMO system has a central frequency of 30 kHz. It is composed of 11 transmitters (Tx) and 11 receivers (Rx) in a "L" shape configuration. The seabed elevation is simulated using fractional Brownian motion model. Simulations were run with a sandy mud seabed type. The average water depth is 15 m.

2 MIMO SYSTEM CALIBRATION

2.1 TRANSDUCER POSITION ACCURACY FOR COHERENT PROCESSING

One of the biggest achievement in the SAS (synthetic aperture sonar) community has been to accurately estimate the platform motion. Micronavigation methods often based on the DPCA[7] (displaced phase-center antenna) concept aim to solve the subwavelength short-term relative platform positioning required for coherent processing.

MIMO and SAS systems share the same principles for synthetic aperture imaging and in both cases back projection algorithms can be applied to produce high resolution images.Therefore even for static

MIMO systems the relative positions between transmitters and receivers has to be known with a subwavelength precision, as illustrated in Figure 1 where a point scatterer is imaged using the back projection technique with different transducer location accuracy.

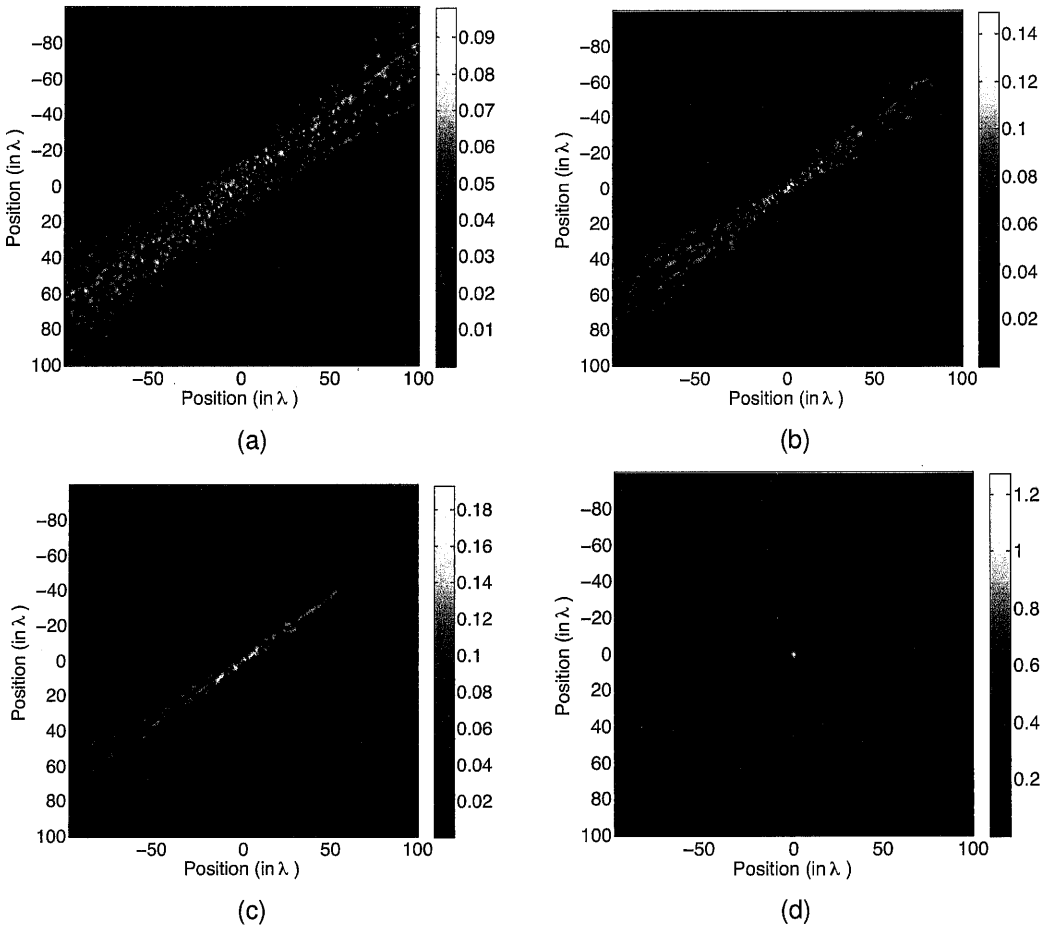

Figure 1: MIMO image of a point scatterer target with different accuracy of the transducer locations: (a) 20λ accuracy, (b) 5λ accuracy, (c) 1λ accuracy and (d) $\lambda/10$ accuracy.

Two interesting parameters can be extracted from the unfocused point scatterer MIMO images. The first parameter can be described as a diffusion parameter. When the transducer position accuracy is above one λ the system is highly incoherent and the energy spreads around the target location. The leaking energy is computed as a function of range from the target position. We then define the diffusion parameter as the half width at half maximum. Note that the diffusion parameter is similar to the full width at half maximum $2\sigma\sqrt{2\ln 2}$ of a Gaussian function with a variance of σ. The second parameter is the maximum amplitude of the scattering point target.

Figure 2(a) and (b) display respectively the diffusion parameter and the maximum amplitude parameter as a function of the Rx/Tx location accuracy. To be noted that the transition between incoherent system and coherent system is clearly visible in Figure 2(b). As the transducer positions reach a subwavelength accuracy the contributing phases of the MIMO pairs add coherently and the maximum target amplitude increases drastically up to $\lambda/10$ where the maximum amplitude stabilises.

2.2 MIMO ARRAY CALIBRATION

Considering the installation of a static MIMO system in an harbour environment, assuming a central frequency of 30 kHz ($\lambda = 5$ cm), one can expect to know the Tx/Rx locations with $10\lambda = 50$ cm

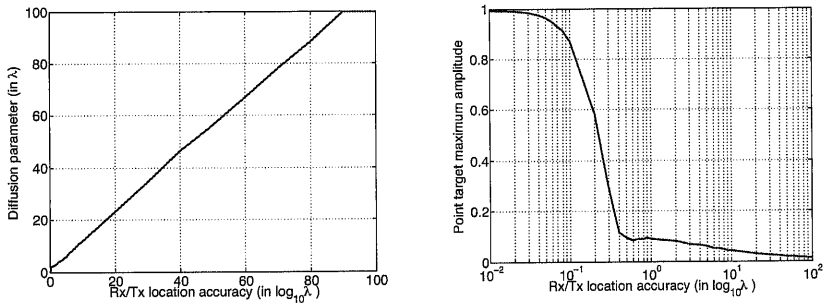

(a) (b)

Figure 2: (a) Diffusion parameter, (b) Maximum amplitude of a point scatterer MIMO image depending on the Rx/Tx location accuracy.

accuracy. Given the results from the previous section the MIMO system cannot be considered as coherent and array calibration is needed to achieve a $\lambda/10$ position accuracy.

To calibrate the MIMO system we assume that a bright scattering point target (calibrating target) is present in the scene and that its position is known with 10λ accuracy. Given a MIMO system with K transmitters and L receivers, the calibration problem consists in finding the $T+R$ transducer locations with an accuracy of $\lambda/10$. Considering the high dimensionality and non convex nature of the problem, we chose a genetic algorithmic approach.

Each candidate solution is represented by the positions of the transmitters and the receivers, $G = \{\{X_k^t\}_{k\in[1,K]}, \{X_l^r\}_{l\in[1,L]}\}$, where X_k^t is the location of the transmitter k and X_l^r is the location of the receiver l. The first population is chosen randomly within the location interval accuracy: $X_n^t \sim \mathcal{U}(X_k^{t0} - 10\lambda, X_k^{t0} + 10\lambda)$, where $\mathcal{U}$ is the uniform distribution and X_k^{t0} is the transducer first location estimation within 10λ.

The fitness functions are the diffusion parameter and the maximum amplitude parameter presented in section 2.1. Note that at first one wants to minimise the diffusion parameter to reach the coherent domain and then maximise the maximum amplitude parameter.

In order to control the algorithm convergence we chose a coarse to fine approach by selecting the following mutation process: each chromosome X_k^t is mutated into $X_k^t + \delta$ where $\delta \sim \mathcal{U}(\epsilon)$. The probability density function (PDF) of the mutated chromosome has then a trapezoid shape (cf. Figure 3). ϵ is chosen such as the interval $[-N+\epsilon, N-\epsilon]$ (highlighted in red in the figure) represents α % of the probability. ϵ is then given by:

$$\epsilon = \frac{2N(1-\alpha)}{\alpha+2} \tag{1}$$

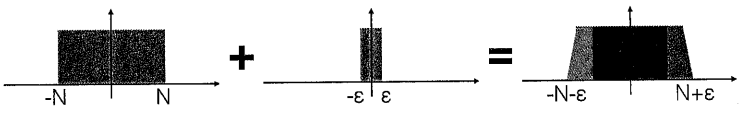

Figure 3: Mutation process: each chromosome is mutated by the addition of $\delta \sim \mathcal{U}(\epsilon)$.

For α =90% the probability that a mutated candidate be within the $[-N+\epsilon, N-\epsilon]$ interval is $\alpha^{T+R} \approx 10\%$. So in our case around 10% of the mutated candidates are uniformly getting closer to the solution. Figure 4 shows the convergence of the algorithm by narrowing progressively the research window interval. Note that Figure 4 shows the upper band of the convergence.

A crossover between candidates is also performed. The crossover candidate $G_c = \text{Crossover}(G_1, G_2)$

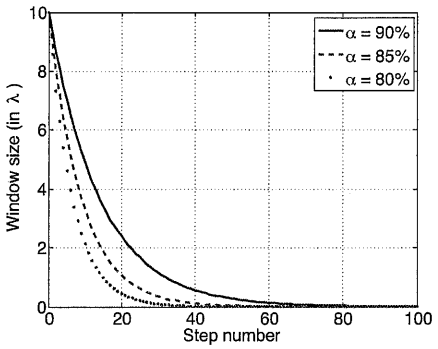

Figure 4: Convergence of the research window interval for different value of α.

is given by $G_c = \{\{(X_k^t + Y_k^t)/2\}_{k\in[1,K]}, \{(X_l^r + Y_l^r)/2\}_{l\in[1,L]}\}$. The crossover operation ensures that a specific gene does not drift apart from the solution when the other genes converge.

Using a population of 200 individuals the proposed calibration algorithm converged to an approximate $\lambda/10$ average position accuracy with a maximum absolute error of $\lambda/5$.

3 SIDELOBES REDUCTION

The consequence of the sparsity of the transmitters and receivers in a distributed MIMO system is an increase of the sidelobe level.

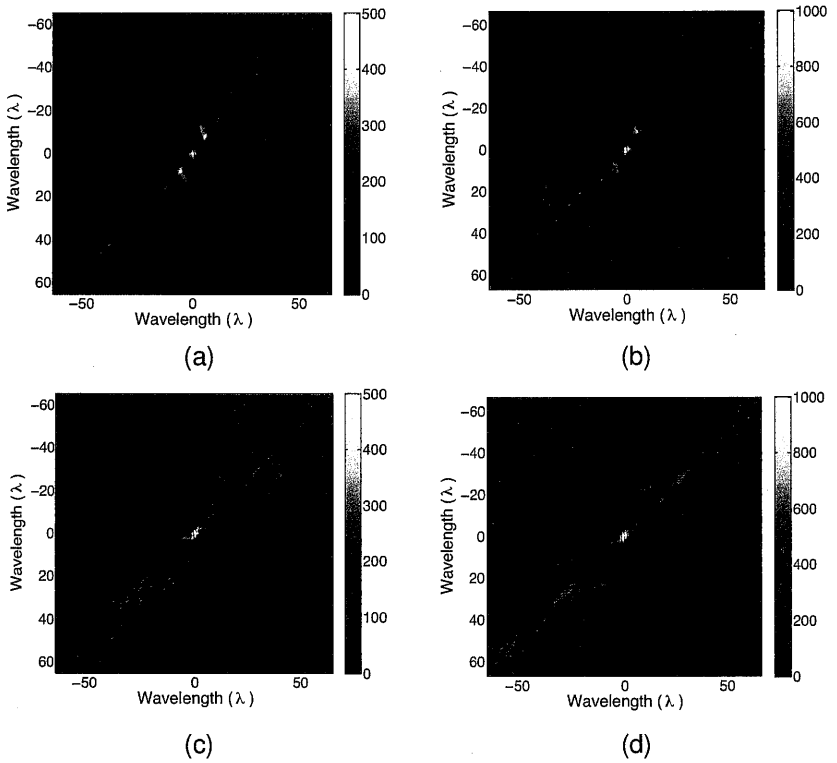

Figure 5: MIMO image of (a) point scatterer with a regular array, (b) 3 point scatterers with a regular array, (c) point scatterer with an optimised random array and (d) 3 points scatterers with an optimised random array.

Figure 5(a) displays a MIMO image of a point scatterer with a regular array: the transmitters and receivers are aligned with a 3 m interval. Important side lobes around 10 dB lower than the target are then clearly visible and can increase the false alarm rate. The sidelobe problem with sparse array is a well known problem and can be solved using random arrays[8] .

Using similar genetic algorithm discussed in section 2.2 adapted to sidelobe reduction it is relatively straightforward to reduce the sidelobe by a factor of 10 dB. Figure 5(c) displays the MIMO image of a point scatterer using an optimised array. The sidelobes are well reduced and with 20 dB lower that the target amplitude are closer to reverberation level.

The main difference between sonar systems and radar systems is the target scattering process. In radar a target is well modelled by a single scattering coefficient[8–10] . This randomness preserves the properties of random arrays. With sonar however a manmade target often shows regularities (translation invariant, rotation invariant etc.). Random arrays cancel the constructive interference of a regular array which create important sidelobes. By introducing a symmetry or a regularity in the target, one can cancel the random array properties. Figure 5(d) highlights this particular point: a 3 point scatterer target is imaged using the MIMO random array optimised for a one point scatterer target. The sidelobes raise from -10 dB to -1.5 dB.

4 AUTOFOCUS WITH MIMO SYSTEMS

The MIMO images are computed using the multistatic back projection algorithm which is a variant of the bistatic back projection algorithm[11] developed by the SAR community. For the multi-static scenario the continuous integration along ellipses is replaced by a finite sum in which each term corresponds to one transmitter/receiver pair contribution. In this section we propose two variants of the multistatic back projection algorithm to estimate the depth of a mid-water target, its speed and orientation.

4.1 DEPTH ESTIMATION

As it has been mentioned before synthetic aperture MIMO imaging shares a lot of features with standard SAS imaging. In particular the image is projected onto a plane or a bathymetry estimate representing the seafloor level. The image of a mid water target will then appear unfocused for this particular projection. By moving the projection plane through the water column the MIMO target image will focus at its actual depth. Using simple autofocus algorithm and maximising the target amplitude it is then possible to estimate the depth of the target even if the MIMO system is coplanar. For a mid-water target at 400 m range in a 15 m depth environment it is possible to estimate its depth with 10 to 50 cm accuracy. Figure 6 displays the autofocus results and the estimated target depth compared with the ground truth.

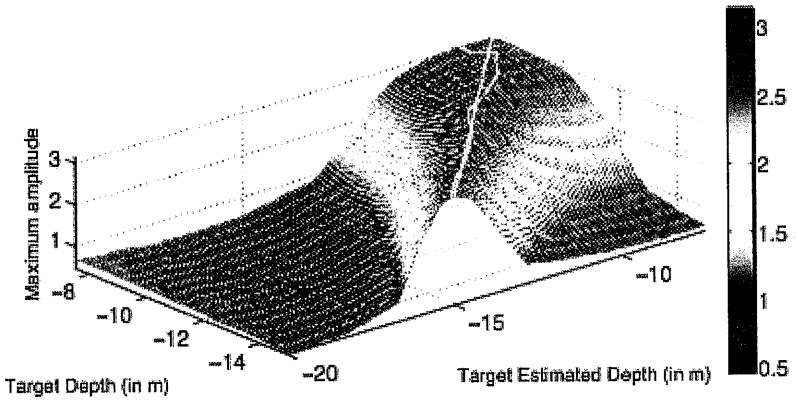

Figure 6: Autofocus algorithm results based on maximising the scattering response: ground truth (white curve) and estimated depth (green curve).

4.2 SPEED AND DIRECTION ESTIMATION

Speed estimation for MIMO systems is an active subject of research in the radar community[9,10] . Most of the proposed methods are based on maximum-likelihood (ML) estimation and then rely on the Doppler shift of the moving target. In our case we are interested in low velocity target (few knots) in a highly cluttered and multiplath environment. For these reasons we assume in this paper that the Doppler shift is negligible.

The main idea of speed and direction autofocus is to introduce a defocus for moving objects and then estimate the speed and direction parameter $\overrightarrow{v}$ which will re-focus the target. In our scenario the MIMO system inspects a 200 m $\times$ 300 m area. In this area we are interested in target travelling at around 1.5 m.s^{-1}. If all the Tx were to transmit at the same time the maximum displacement of the target relative to all the transmitted pulses would be in the order of $\lambda/10$. Figure 7(b) displays the MIMO image with no transmitting delay of a target moving at 1.5 m.s^{-1}. In agreement with the results from section 2.1 the image of the target is still well focused.

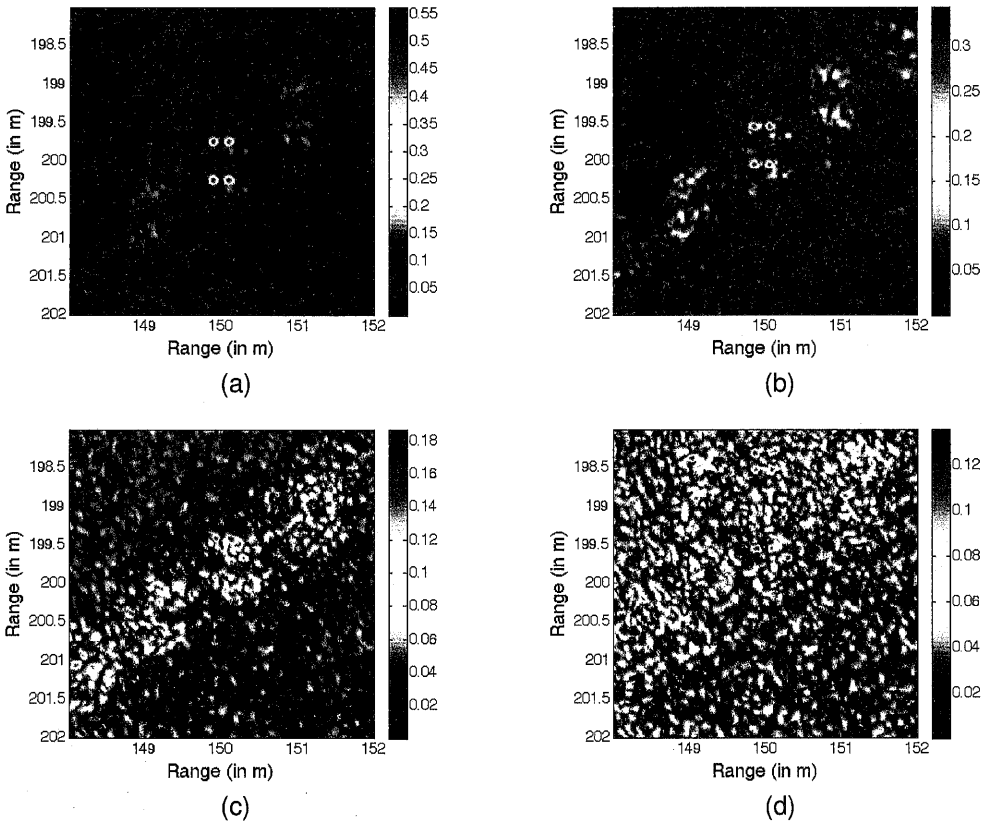

Figure 7: MIMO image of (a) a static target, (b) moving target with no transmitting delay, (c) moving target with random transmitting delay introducing an average of $4\lambda/5$ target displacement and (d) moving target with random transmitting delay introducing an average of 10λ target displacement.

By introducing random delays to the transmitting pulses we can control the average time difference Δt between pulse times of arrival at the target. The target will then move between two pulses by $\overrightarrow{v}\Delta t$ on average. Figure 7(c) and (d) display the MIMO image of a moving target with random transmitting delay introducing respectively $4\lambda/5$ and 10λ displacement. For a high displacement (greater than λ) the resulting target image is not coherent anymore. For low reflectivity targets the target signal can then be masked by the reverberation level (cf. Figure 7(d)). For an average displacement lower than λ the back projection processing is still coherent and the target structure visible (cf. Figure 7(c)).

From the defocused image and assuming a constant velocity it is possible to compensate the target

motion by time shifting the MIMO responses. Let note $z_{kl}(t)$ the signal recorded at the receiver l from the transmitter k. Let note $\Delta_k t$ the transmitting delay of the transmitter k and d_k the distance between transmitter k and the target. The target displacement from $t = 0$ to $t = \delta t = \Delta_k + d_k/c$ time where the pulse transmitted by the transmitter k hit the target is $\overrightarrow{v}\delta t$. The path difference Δ_{kl} between the target location at $t = 0$ and the target location at $t = \delta$ is then:

$$\Delta_{kl}(\overrightarrow{v}) = (\overrightarrow{u_k} + \overrightarrow{u_l}).\overrightarrow{v}\delta t = (\Delta_k + d_k/c)(\overrightarrow{u_k} + \overrightarrow{u_l}).\overrightarrow{v} \tag{2}$$

where $\overrightarrow{u_k}$ and $\overrightarrow{u_l}$ are respectively the direction of arrival and the direction of departure of the sound wave from the target coordinates. Figure 8 draws a schematic of the configuration.

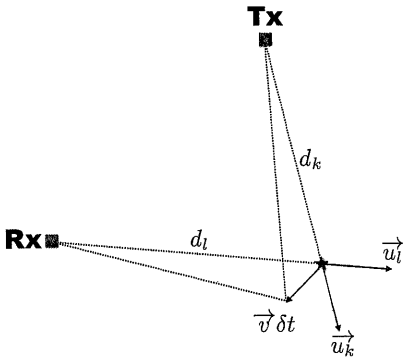

Figure 8: Schematic and notations: path difference of a moving target.

To focus at a velocity $\overrightarrow{v}$ we then need to compensate for the transmitting time delay and the target motion by applying the multi static back projection algorithm to the set of signals $\left\{z_{kl}(t - \Delta_{kl}(\overrightarrow{v})/c)_{k,l\in[1,K]\times[1,L]}\right\}$ instead of $\left\{(z_{kl}(t))_{k,l\in[1,K]\times[1,L]}\right\}$. The estimated velocity $\overrightarrow{v_e}$ is then given by:

$$\overrightarrow{v_e} = \max_{\overrightarrow{v}}\left[\max\left(\mathrm{BP}\left(\left\{z_{kl}(t - \Delta_{kl}(\overrightarrow{v})/c)\right\}_{k,l\in[1,K]\times[1,L]}\right)\right)\right] \tag{3}$$

where BP is the multi static back projection image formation. Figure 9 display the $\max(\mathrm{BP}(\overrightarrow{v}))$ functions for (a) no transmit delay, (b) $\lambda/4$ displacement transmit delay and (c) $4\lambda/5$ displacement transmit delay. Let note $\overrightarrow{v} = (v, \theta)$ where v is the target speed and θ the target heading.

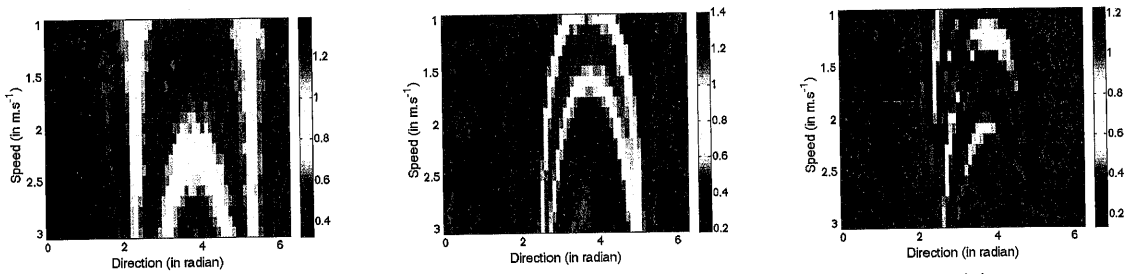

Figure 9: $\max\left(\mathrm{BP}(v, \theta)\right)$ functions for (a) no transmit delay, (b) $\lambda/4$ displacement transmit delay and (c) $4\lambda/5$ displacement transmit delay. v is the target speed in m.s^{-1} and θ the direction in radian.

For no transmit delay or small displacement transmit delay (cf. Figure 9(a) and (b)) the ambiguity between speed and direction is important. In that case the MIMO moving target image was already close to focus and it is not surprising that a large portion of the (v, θ) plane can focus the moving

target image. When the displacement transmit delay is important enough to create a defocusing of the moving target (cf. Figure 7(c)) then the optimal focusing value $\overrightarrow{v}$ is a better constraint (cf. Figure 9(c)).

Around 500 tests for speed and direction estimation have be run using this autofocusing technique. Several types of point targets have been tested in different locations with speeds varying from 0.5 m.s^{-1} to 3 m.s^{-1}. In average the speed is estimated with around 0.15 m.s^{-1} error and the heading with around 6° error.

5 CONCLUSIONS

In this paper we define the limits in terms of transducer location accuracy in which a sonar MIMO system is coherent and can therefore provide super-resolution images. We propose a calibration method involving genetic algorithm in which we were able to control the convergence. We show that the calibration algorithm converges to an average transducer location accuracy of less than $\lambda/10$. Finally we propose two MIMO autofocus techniques enabling to find with great accuracy the depth of a mid-water target and the speed and heading of a moving target.

ACKNOWLEDGEMENTS

This work was supported by the Engineering and Physical Sciences Research Council (EPSRC) Grant number EP/J015180/1 and the MOD University Defence Research Collaboration in Signal Processing.

REFERENCES

[1] A. Haimovich, R. Blum, and L. Cimini. Mimo radar with widely separated antennas. *Signal Processing Magazine, IEEE*, 25(1): pp. 116–129, 2008.

[2] F. Ehlers. *Final report on deployable multistatic sonar systems.* Tech. report, NATO Undersea Research Centre, 2009.

[3] M. Fewell and S. Ozols. *Simple Detection-Performance Analysis of Multistatic Sonar for Anti-Submarine Warfare.* Tech. report, DSTO Defence Science and Technology Organisation, 2011.

[4] Y. Pailhas, Y. Petillot, C. Capus, and B. Mulgrew. Target detection using statistical mimo. In *European Conference on Underwater Acoustics, ECUA12*, 2012.

[5] Y. Pailhas and Y. Petillot. Independent views in mimo sonar systems. In *Underwater Acoustics conference, UA2014*, 2014.

[6] Y. Pailhas, E. Delande, J. Houssineau, Y. Petillot, and D. Clark. Tracking underwater objects using large mimo sonar systems. In *Underwater Acoustics conference, UA2014*, 2014.

[7] A. Bellettini and M. Pinto. Theoretical accuracy of synthetic aperture sonar micronavigation using a displaced phase-center antenna. *Oceanic Engineering, IEEE Journal of*, 27(4): pp. 780–789, Oct 2002.

[8] M. Haleem, A. Haimovich, and R. Blum. Sidelobe mitigation in mimo radar with multiple subcarriers. In *Radar Conference, 2009 IEEE*, pp. 1–6, May 2009.

[9] H. Qian, R. Blum, and A. Haimovich. Noncoherent mimo radar for location and velocity estimation: More antennas means better performance. *Signal Processing, IEEE Transactions on*, 58(7): pp. 3661–3680, July 2010.

[10] A. Hassanien, S. Vorobyov, and A. Gershman. Moving target parameters estimation in noncoherent mimo radar systems. *Signal Processing, IEEE Transactions on*, 60(5): pp. 2354–2361, May 2012.

[11] A. Home and G. Yates. Bistatic synthetic aperture radar. *IEEE RADAR 2002*, : pp. 6–10, 2002.